attenuation of more than 50 dB for 40 to 60 GHz, the measured minimum insertion loss is 1.8 dB. Since the higher order mode excitation and finite thickness of the insert are included in the calculations, the measurements agree well with theory.

Appendix

Coupling Integrals due to the Orthogonal Expansion

$$F^{\mathrm{IV}}_{(mn)} = \int_0^c \sin\left(\frac{m\pi}{a}x\right)\sin\left(\frac{n\pi}{c}y\right)dx$$

$$F^{\mathrm{III}}_{(mq)} = \int_f^a \sin\left(\frac{m\pi}{a}x\right)\sin\left(\frac{q\pi}{a-f}\cdot(x-f)\right)dx$$

$$F^{\mathrm{II}}_{(mk)} = \int_d^e \sin\left(\frac{m\pi}{a}x\right)\sin\left(\frac{k\pi}{e-d}\cdot(x-d)\right)dx.$$

Scattering Coefficients in (6)

$$(S)_{11} = (S)_{12} = \left\{I+U-W(I+U)^{-1}W\right\}^{-1} \cdot \left\{I-U-W(I+U)^{-1}W\right\}$$

$$(S)_{12} = (S)_{21} = \left\{I+U-W(I+U)^{-1}W\right\}^{-1} \cdot W\left\{U-(I+U)^{-1}(I-U)\right\}$$

where

$$I = \sum_{\nu=\mathrm{II}}^{\mathrm{IV}} L^{\nu}_E\left\{U+2D^{\nu}(U-D^{\nu}D^{\nu})^{-1}D^{\nu}\right\}L^{\nu}_H$$

$$W = \sum_{\nu=\mathrm{II}}^{\mathrm{IV}} 2L^{\nu}_E D^{\nu}(U-D^{\nu}D^{\nu})^{-1}L^{\nu}_H$$

with

U unit matrix,

D^{ν} diagonal matrix of the eigenmodes (also below their cutoff frequency) along the waveguide sections i between the step discontinuities

$$D^{\nu}_{(mm)} = e^{-jk^{\nu}_{z(m)}\cdot l_i}$$

$$L^{\mathrm{IV}}_{E(mn)} = 2\sqrt{\frac{k^{\mathrm{I}}_{z(m)}}{a\cdot c\cdot k^{\mathrm{IV}}_{z(n)}}}\cdot F^{\mathrm{IV}}_{(mn)}$$

$$L^{\mathrm{II}}_{E(mk)} = 2\sqrt{\frac{k^{\mathrm{I}}_{z(m)}}{a(e-d)k^{\mathrm{II}}_{z(k)}}}\cdot F^{\mathrm{II}}_{(mk)}$$

$$L^{\mathrm{III}}_{E(mq)} = 2\sqrt{\frac{k^{\mathrm{I}}_{z(m)}}{a(a-f)k^{\mathrm{III}}_{z(q)}}}\cdot F^{\mathrm{III}}_{(mq)}$$

$$\left(L^{\nu}_H\right) = \left(L^{\nu}_E\right)^T, (T = \text{transposed}).$$

Acknowledgment

The authors wish to thank Dr. Rembold, the head of the microwave laboratory of AEG Telefunken, Ulm, West Germany, and the members of his staff, especially Dr. Menzel, for helpful discussions and financial support of this work.

References

[1] P. J. Meier, "Integrated fin-line millimeter components," *IEEE Trans. Microwave Theory Tech.*, vol. MTT-22, pp. 1209–1216, Dec. 1974.

[2] F. Arndt, J. Bornemann, D. Grauerholz, and R. Vahldieck, "Low-insertion loss fin-line filters for millimeter-wave applications," in *Proc. 11th European Microwave Conf.*, Amsterdam, 1981, pp. 309–314.

[3] ———, "Theory and design of low-insertion loss fin-line filters," *IEEE Trans. Microwave Theory Tech.*, vol. MTT-30, pp. 155–163, Feb. 1982.

[4] Y. Konishi and K. Uenakada, "The design of a bandpass-filter with inductive strip—Planar circuit mounted in waveguide," *IEEE Trans. Microwave Theory Tech.*, vol. MTT-22, pp. 869–873, Oct. 1974.

[5] R. Vahldieck, J. Bornemann, F. Arndt, and D. Grauerholz, "Optimized waveguide *E*-plane metal insert filters for millimeter-wave applications," *IEEE Trans. Microwave Theory Tech.*, vol. MTT-31, pp. 65–69, Jan. 1983.

[6] Y.-C. Shi, T. Itoh, and L. Q. Bui, "Computer-aided design of millimeter-wave *E*-plane filters," *IEEE Trans. Microwave Theory Tech.*, vol. MTT-31, pp. 135–141, Feb. 1983.

[7] H. Patzelt and F. Arndt, "Double-plane steps in rectangular waveguides and their application for transformers, irises, and filters," *IEEE Trans. Microwave Theory Tech.*, vol. MTT-30, pp. 771–776, May 1982.

A Comparison of IMPATT Oscillator Power and Frequency Above 100 GHz with Results Derived from Theoretical Models

BEVAN D. BATES, MEMBER, IEEE

***Abstract*—A comparison is made of experimentally determined IMPATT oscillator frequency and power characteristics in the 90–140-GHz band with values obtained from detailed theoretical models. The results show encouraging agreement and demonstrate the potential of the modeling approach for oscillator design.**

I. Introduction

This paper compares measured 117-GHz IMPATT oscillator frequency and output power with results derived from theoretical circuit models. Previous millimeter-wave oscillator models reported in the literature either rely on small-signal device models [1], [2] and therefore cannot yield output power, or use elementary circuit models [3] and are thus unsuitable for studying circuit behavior, such as oscillator tuning as a function of waveguide short position or other circuit parameters. In this paper, oscillator circuit modeling techniques, successfully applied at *X*-band [4], [5], are applied for the first time to a millimeter-wave IMPATT oscillator circuit.

II. Oscillator Circuit Description

The circuit under consideration, shown in Fig. 1, is of the cross-coupled coaxial/waveguide type, constructed in half-height waveguide with a linearly tapered transition to full-height waveguide at the output. The IMPATT diode, mounted on a copper heatsink in a double-quartz-standoff package, is soldered to a copper post and inserted in the lower coaxial section and contacted by the coaxial center conductor. The other end of the coaxial line is terminated at RF by a section of Eccosorb[1]

Manuscript received October 24, 1983; revised April 13, 1984. This work was supported by a National Research Council Resident Research Associateship at the Jet Propulsion Laboratory, Pasadena, CA, under contract with the National Aeronautics and Space Administration.

The author is with the Department of Electrical and Electronic Engineering, University of Melbourne, Parkville, Vic., 3052, Australia. He was an NRC-NASA Resident Research Associate at the Jet Propulsion Laboratory, 4800 Oak Grove Drive, Pasadena, CA 91109.

[1]Emerson and Cuming, Inc

0018-9480/84/1000-1394$01.00 ©1984 IEEE

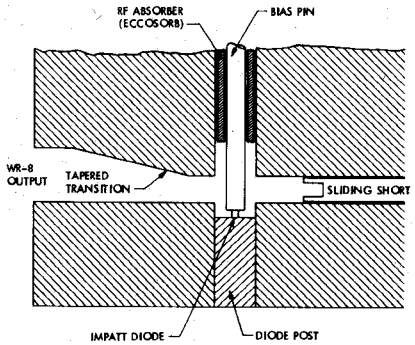

Fig. 1. IMPATT oscillator mount cross section.

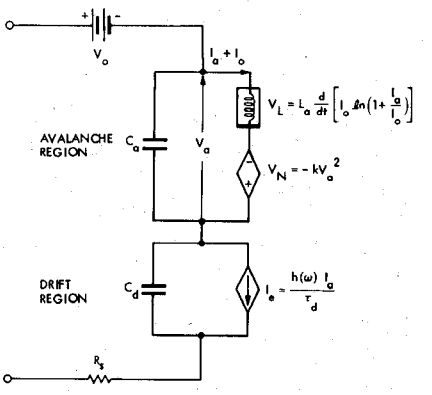

Fig. 2. IMPATT diode circuit model.

absorber whose position relative to the diode is adjustable for tuning purposes. The Eccosorb section also functions as a low-pass filter through which a constant-current dc bias is applied to the diode. A micrometer-driven contacting backshort terminates the other waveguide port.

III. Diode Model

The IMPATT diode circuit model shown in Fig. 2 is derived from the nonlinear model of Gannett and Chua [6]. This model is a significant improvement over other IMPATT circuit models for use at millimeter-wave frequencies because it includes a distributed drift-region model and the effect of diffusion is accounted for in both the avalanche and drift regions. The model may be viewed as a more accurate representation of the original analysis of Read [7]. Application at millimeter-wave frequencies is limited by the quasistatic assumption; i.e., the time variations of physical variables are assumed "slow" compared with the avalanche-region transit time. In highly doped n-type silicon, as is frequently used for millimeter-wave IMPATT devices, the avalanche region is typically 45 percent of the total depletion-layer width [8], and thus the quasistatic assumption is less accurate than in p-type silicon with an avalanche-width ratio of 25 percent at the same doping density. Because of this limitation and difficulties in nonlinear computation, not all of the second-order features of the Gannett and Chua model were included. However, diffusion effects were included and an effective ionization rate was used to account for the differing ionization rates of electrons and holes in silicon. This IMPATT circuit model is believed to be the best available without resorting to large-scale numerical simulations which require considerable computation and are thus less suitable for circuit studies.

The model parameters required (apart from the material properties) are the junction area, the avalanche-region width, and the drift-region width. For an abrupt junction, these parameters are estimated from the voltage and junction capacitance at breakdown for the reverse-biased diode with the aid of published curves [8]. Capacitance versus voltage ($C-V$) measurements provide a simple means of confirming an abrupt junction in a single-drift-region device. More sophisticated methods, such as secondary ion mass spectroscopy analysis, may be used to determine the doping profile in double-drift-region devices or devices with arbitrary doping profiles.

The following parameters were determined for a single-drift-region n-type device designed for CW operation near 140 GHz. The breakdown voltage was 10.0 V, which yielded a doping density of 1.2×10^{17} cm^{-3}, a total depletion-layer width of 0.3 μm and an avalanche-width fraction of 45 percent. A least-squares fit to the measured $C-V$ curve yielded a zero-bias capacitance of 1.4 pF, a nonlinearity index of 0.53 (cf., 0.5 for an abrupt junction) and a contact potential of 0.92 V. From these parameters, the capacitance at breakdown was calculated to be 0.37 pF. Using this value, together with the depletion-layer width of 0.3 μm, gave a junction area of 1.1×10^{-5} cm^2, corresponding to a diameter of 37 μm. These parameters agree favorably with published data for similar diodes [9, table I]. The diode series resistance was estimated to be 0.35 Ω using the oscillation-threshold method of Alderstein *et al.* [10]. The parameters of the diode model at 300 mA dc bias are summarized in Table I.

TABLE I
Diode Parameters for Fig. 2

PARAMETER	VALUE
Breakdown voltage, V_0	9.7 V
DC bias current, I_0	.3 A
Avalanche current, I_a	.25 A+
Avalanche voltage, V_a	.61 V+
Avalanche capacitance, C_a	.82 pF
Drift capacitance, C_d	.65 pF
Avalanche inductance, L_a (small signal value)	3.01 pH
Voltage source constant, k	.178 V^{-1}
Drift region transfer function, $h(\omega)/\tau_d$	.646 -j.507*
Series resistance, R_s	.35 Ω

+ Typical value

* Frequency dependent. Value at 117 GHz

IV. Circuit Model

The oscillator circuit model was derived from the work of Williamson [11] and Allen, Bates, and Khan [5]. Allen *et al.* extended the Williamson analysis to account for higher order mode propagation in the waveguide and distributed loss in the waveguide and coaxial line. The result is an equivalent circuit of the junction from which the impedance at any port may be readily calculated, given the terminating impedances on the other ports. Experimental measurements at X-band [5] have showed this analysis to be more accurate than that of Chang and Ebert [2]. Because the diameter of the coaxial center-conductor is a significant fraction of a wavelength, the driving-point impedance is modified by the radial-line region surrounding the diode. This region is modeled with lumped-element low-pass II sections using the method of Steer and Khan [12]. The impedance presented at the diode wafer is further modified by the diode

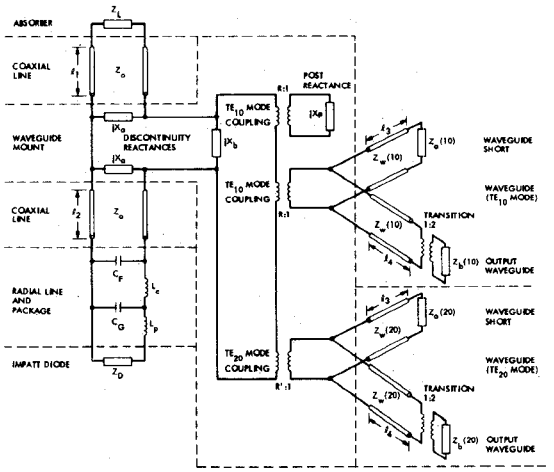

Fig. 3. Oscillator circuit model.

TABLE II
CIRCUIT PARAMETERS FOR FIG. 3

PARAMETER	VALUE
ℓ_1	0.0 in.
ℓ_2	0.0 in.
ℓ_3	.135 in.+
ℓ_4	.03 in.
Z_0	32.9 Ω
Z_L	40.0 Ω
jX_a	-57.3 Ω*
jX_b	57.2 Ω*
jX_p	-65.4 Ω*
$Z_w(10)$	242 Ω*
$Z_w(20)$	j123 Ω*
$Z_a(10)$, $Z_a(20)$	0 Ω
$Z_b(10)$, $Z_b(20)$	Matched Load
R	.859*
R'	.17 x 10-8*
C_F	.032 pF
L_C	.022 nH
C_G	.070 pF
L_p	.021 nH

+ Varies with short position

* Frequency dependent. Value at 117 GHz

package which, as usual, is considered part of the external oscillator circuit and modeled by a simple $L-C$ section. The complete circuit model is shown in Fig. 3, and typical values for the circuit elements are given by Table II.

One problem that arises in characterizing this circuit is that little is known about the impedance of the Eccosorb termination at millimeter-wave frequencies. Because a flat (rather than tapered) termination is used, and its relative position has a considerable influence on the output power of the oscillator, the termination must be mismatched. Use of a mismatched termination is known to be advantageous in the operation of similar oscillator circuits [2] as it provides a convenient method of optimizing the output power. However, as the magnitude of this mismatch cannot be easily measured at millimeter-wave frequencies, the low-frequency VSWR of 1.2 was assumed for the analysis.

V. Oscillator Analysis

Oscillator frequency and output power were determined at operating points found from the Kurokawa condition [13], $Z_D + Z_C = 0$ where Z_D is the diode impedance and Z_C is the circuit impedance. Z_D is a function of both oscillation amplitude and frequency, while Z_C is a function of frequency only. The operating point is found using a Fletcher–Powell search method [14] to minimize an appropriately chosen objective function such that a minimum of zero indicates a solution to $Z_D + Z_C = 0$. The Kurokawa stability criterion indicates if this solution is a possible operating point.

VI. Results and Discussion

Measurements were made of the oscillator frequency and output power as a function of backshort position and bias current. The absorber and diode positions were adjusted to give the broadest mechanical tuning range. Best performance was generally obtained with both the diode and the absorber almost flush with the waveguide walls such that the lengths of the upper and lower coaxial line sections were almost zero.

The measured values of frequency and output power as a function of dc-bias current are shown in Fig. 4 compared with the values calculated from the theoretical models discussed in Sections III and IV. The backshort position was 0.09 in. The calculated frequency differs from the measured frequency by 2 GHz or less and is independent of bias current, while the measured frequency shows a slight bias-current dependency. The calculated output power shows a greater sensitivity to bias current than the measured output power. The calculated threshold is 270 mA compared with the experimental value of 235 mA, while the calculated power is 6 dB greater at the bias current of 400 mA at which output power saturates. The measured and calculated values of frequency and output power at 300 mA dc bias as a function of backshort position are shown in Fig. 5. The calculated frequency (Fig. 5(a)) agrees favorably with the experimental values, particularly with regard to slope. However, the calculated frequency is again generally about 2 GHz above the measured value, and the tuning range of each longitudinal mode in Fig. 5 is approximately half the observed value (7 GHz rather than 14 GHz). The calculated power output agrees well with the experimental values (Fig. 5(b)) with respect to the maximum power and the backshort position (and therefore frequency) at which this maximum occurs. However, the calculated output power decreases more rapidly either side of this maximum than the measured power.

The discrepancy in frequency is most easily explained by an apparent shift of 0.005 in in the position of the backshort. Although careful attention was given to the construction of the backshort, a difference of 0.005 in between the physical and electrical planes of the short circuit is within the limits of accuracy expected from a contacting short [2]. The discrepancy in tuning range is better understood in relation to the output power characteristic. The calculated tuning range is limited at the high-frequency end by the small-signal negative-resistance of the diode becoming insufficient to sustain oscillation, while at the low-frequency end the oscillation becomes unstable. The instability occurs because both the diode resistance and reactance are changing rapidly as oscillation frequency approaches the calculated diode avalanche-resonance frequency of 101.2 GHz. Because the power is determined primarily by the condition that the sum of the real parts of the diode and circuit impedances be zero (while the frequency is determined primarily by the zero condition on the imaginary parts), the modeling of the resistive parts of the diode and circuit impedances is of major importance.

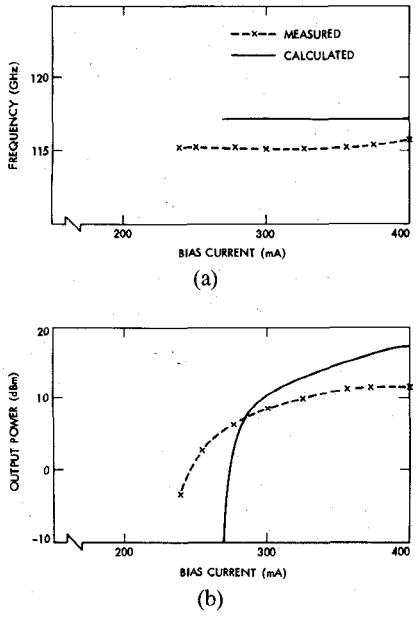

Fig. 4. Measured and calculated (a) frequency and (b) output power as a function of diode bias current.

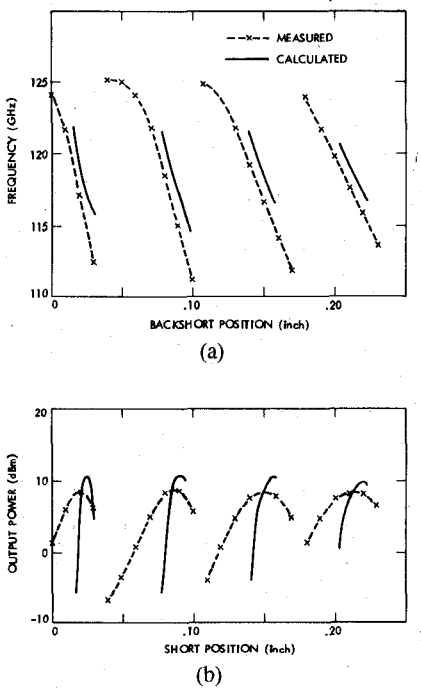

Fig. 5. Measured and calculated (a) frequency and (b) output power as a function of waveguide short position.

First consider the diode model. The most likely source of the discrepancy in output power is in the breakdown of the quasi-static assumption. Because the avalanche-region width is approaching half the total depletion-layer width, avalanche-region transit times are significant and thus the device cannot be accurately divided into separate "avalanche" and "drift" regions. However, an alternate modeling approach yielding greater accuracy may also require intensive numerical calculations and thus be inconsistent with the oscillator analysis approach used in this paper to find the operating point.

Other sources of discrepancy in the calculated output power are uncertainties in appropriate values for material parameters at the high frequencies and electric fields encountered in the millimeter-wave devices. Important parameters which affect the diode negative resistance are the ionization rates and diffusion constants. Although the ionization rates of Grant [15] are known to be more accurate than those of Lee *et al.* [16], the Lee rates were used because the curves from which the diode parameters were determined used these rates [8]. The diffusion constants used were the low field values of 18.2 cm^2/s for electrons and 6.5 cm^2/s for holes.

The major uncertainties in the waveguide circuit model are the values of the diode package inductance and the Eccosorb termination impedance. These values were estimated based on low-frequency data. However, the package inductance does not affect the real part of the mount impedance and thus only indirectly affects the output power (by changing the oscillation frequency). Changes in the Eccosorb termination impedance affect the output power in two ways: first, by changing the impedance presented to the diode, and second, by changing the circuit efficiency, defined as the ratio of useful power delivered to the waveguide load to the sum of this power and the power lost in Eccosorb termination. The output power is less sensitive to the magnitude of the VSWR of the termination than to the phase (and hence to the termination position), but the sensitivity to both increases with VSWR. Although not considered in this analysis, the impedance of the termination at harmonic frequencies can significantly affect the output power [5].

Another possible source of discrepancy between measured and calculated frequency and output power is in the modeling of the coaxial-to-waveguide junction. Although distributed loss in both the waveguide and coaxial-line sections and higher order waveguide modes have been accounted for in the model, nonidealities in the junction that have not been modeled include: eccentricity in the coaxial line, nonuniformity of waveguide dimensions, surface roughness, and higher order coaxial modes. These nonidealities arise largely because of difficulties in fabricating the circuit to the close tolerances required in millimeter-wave circuits. The tapered transition was also assumed to be an ideal impedance transformer.

Note that the theoretical results presented here were obtained directly from circuit models of the diode and oscillator circuit. The only measurements necessary to obtain the theoretical predictions were the dc breakdown voltage and $C-V$ curve for the diode. The only estimated parameters were the package inductance and the terminating impedance of the coaxial line. Thus, the methods used here can form the basis of an oscillator design approach. It should also be noted that the output power is sensitive to small changes in the diode negative resistance because the magnitude of this resistance ($\sim 2\ \Omega$) is small compared with the output waveguide impedance ($\sim 120\ \Omega$). A change of 10 percent in the diode resistance will typically cause a change of more than 10 dB in the oscillator output power. Thus, accurate prediction of output power requires accurate knowledge of the resistance of the diode and associated series resistances.

VII. Conclusion

A comparison has been made of theoretically derived IMPATT oscillator characteristics with measured data. The results show that useful agreement can be obtained in output power as well as frequency. Improvements in accuracy require refinement of diode and circuit models and a better knowledge of material properties appropriate to millimeter-wave frequencies.

Acknowledgment

The author is grateful to W. Wilson and P. Khan for helpful suggestions, P. Allen and M. Steer for assisting with computer programs, A. Braley for circuit fabrication, and H. Yen of the

Electron Dynamics Division, Hughes Aircraft Company, for supplying the diodes.

References

[1] T. T. Fong, K. P. Weller, and D. L. English, "Circuit characterization of *V*-band IMPATT oscillators and amplifiers," *IEEE Trans. Microwave Theory Tech.*, vol. MTT-24, pp. 752–758, Nov. 1976.

[2] K. Chang and R. L. Ebert, "*W*-band power combiner design," *IEEE Trans. Microwave Theory Tech.*, vol. MTT-28, pp. 295–305, Apr. 1980.

[3] L. H. Holway and S. L. Chu, "Broad-band characteristics of EHF IMPATT diodes," *IEEE Trans. Microwave Theory Tech.*, vol. 30, pp. 1933–1939, Nov. 1982.

[4] B. D. Bates and P. J. Khan, "Analysis of waveguide IMPATT oscillator circuits," in *1981 IEEE/MTT-S Int. Microwave Symp. Dig.*, pp. 232–234, June 1981.

[5] P. J. Allen, B. D. Bates, and P. J. Khan, "Analysis and use of Harkless diode mount for IMPATT oscillators," in *1982 IEEE/MTT-S Int. Microwave Symp. Dig*, June 1982, pp. 138–141.

[6] J. W. Gannett and L. O. Chua, "A nonlinear circuit model for IMPATT diodes," *IEEE Trans. Circuits Syst.*, vol. CAS-25, pp. 299–308, May 1978.

[7] W. T. Read, "A proposed high-frequency negative-resistance diode," *Bell Syst. Tech. J.*, vol. 37, pp. 401–466, Mar 1958.

[8] W. E. Schroeder and G. I. Haddad, "Avalanche region width in various structures of IMPATT diodes," *Proc. IEEE*, vol. 59, pp. 1245–1248, Aug. 1971.

[9] K. Chang, W. F. Thrower, and G. M. Hayashibara, "Millimeter-wave silicon IMPATT sources and combiners for the 110–260-GHz range," *IEEE Trans. Microwave Theory Tech.*, vol. MTT-29, pp. 1278–1284, Dec. 1981.

[10] M. G. Alderstein, L. H. Holway, Jr., and S. L. G. Chu, "Measurement of series resistance in IMPATT diodes," *IEEE Trans. Electron Devices*, vol. ED-30, pp. 179–182, Feb. 1983.

[11] A. G. Williamson, "Analysis and modeling of 'two-gap' coaxial line rectangular waveguide junctions," *IEEE Trans. Microwave Theory Tech.*, vol. MTT-31, pp. 295–302, Mar. 1983.

[12] M. B. Steer and P. J. Khan, "Wideband equivalent circuits for radial transmission lines," *Inst. Elec. Eng. Proc.*, vol. 128, Pt. H, pp. 111–113, Apr. 1981.

[13] K. Kurokawa, "Some basic characteristics of broadband negative resistance oscillator circuits," *Bell Syst. Tech. J.*, vol. 48, pp. 1937–1955, Aug. 1969.

[14] Harwell Subroutine Library, routine VA09A.

[15] W. N. Grant, "Electron and hole ionization rates in epitaxial silicon at high electric fields," *Solid-State Electron.*, vol. 16, pp. 1189–1203, 1973.

[16] C. A. Lee, R. A. Logan, R. L. Batdorf, J. J. Kleimack, and W. Wiegmann, "Ionization rates of holes and electrons in silicon," *Phys. Rev.*, vol. 134, pp. A761–A773, May 1973.

Generation of High-Frequency Radiation by Quasi-Optical Gyrotron at Harmonics of the Cyclotron Frequency

BARUCH LEVUSH AND WALLACE M. MANHEIMER

Abstract—**A quasi-optical gyrotron can operate, in principle, at high harmonics of the electron-cyclotron frequency, as well as at the fundamental. Lower harmonics are suppressed by exploiting their larger diffraction losses. The radiation-field amplitude is kept below the breakdown value by taking advantage of the focusing properties of the quasi-optical resonator. Cavity design parameters and starting currents are presented which characterize the operation of the quasi-optical gyrotron at the eighth harmonic of gyrofrequency.**

Manuscript received November 14, 1983; revised April 16, 1984. This work was supported by the Office of Naval Research.

B. Levush is with the Laboratory for Plasma and Fusion Energy Studies, University of Maryland, College Park, MD 20742.

W. M. Manheimer is with the Naval Research Laboratory, Washington, D.C.

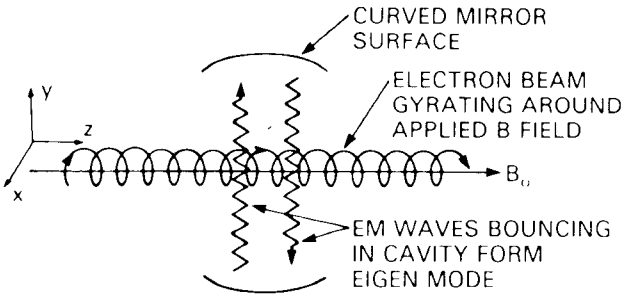

Fig. 1. A quasi-optical gyrotron configuration with the magnetic field in the z direction and the radiation bouncing back and forth in the y direction with its electric-field polarization in the x direction.

I. Introduction

Presently, one of the main efforts in gyrotron research is concerned with further shortening the wavelength of the radiation. To this end, there has been interest in extrapolating gyrotron operation to higher frequencies by utilizing a confocal quasi-optical cavity [1]–[9]. Here, an electron beam travels along a magnetic field perpendicular to the axis of an optical cavity as shown in Fig. 1. In order to operate at higher frequencies, one could envision working at a higher magnetic field or operating at harmonics of the cyclotron frequency. The latter method has been analyzed in a quasi-optical cavity in both a time-independent [1]–[9] and a multimode time-dependent [5]–[8] regime. It has been shown [5]–[7] that, with suitable contouring of the dc magnetic field, a stable single-mode operation of the device at fundamental [5]–[7] and second harmonic of gyrofrequency [8] is possible.

This paper shows that very high cyclotron-frequency harmonics operation is possible in a quasi-optical gyrotron. Although we only consider single-cavity gyrotron configurations with uniform magnetic fields here, it is reasonably clear from earlier work that the efficiency and coherence of the devices could be improved by contouring the guide field and/or by utilizing a double-cavity klystron configuration. Using this scheme, coherent radiation can be produced with power levels of several kilowatts (with efficiency of several percent) at wavelengths ranging from 3 mm, using a permanent magnet, down to 130 μm, using a Nb_3Sn superconducting magnet. The beam energy is typically 260 kV and current $I \simeq 1$ A. This voltage is larger than typical gyrotron voltages, but is still small enough to be available commercially [10].

This investigation is an extension of our earlier work [9] which showed how to select cavity parameters for second- and third-harmonic operation. Here, we show that the same considerations can be applied to much higher harmonic operation. In a quasi-optical configuration, all harmonics are eigenfunctions of the cavity; therefore, the problem is to select cavity and beam parameters so as to achieve reasonable efficiency and coherent oscillation (i.e., suppression of lower harmonics) at the desired frequency. In Section II, we review linear efficiency and suppression of lower harmonics in the optical resonator. In Section III, we calculate specific beam and cavity parameters for gyrotron operation at the eighth harmonic of gyrofrequency.

II. Beam and Cavity Parameters for High-Harmonic Quasi-Optical Gyrotron Operation

We now utilize the technique developed in [9] to describe the interaction of a beam with the wave field in the quasi-optical

0018-9480/84/1000-1398$01.00 ©1984 IEEE